Bulletin of the Seismological Society of America, Vol. 81, No. 2, pp. 468–490, April 1991

GEOLOGICAL CONSTRAINTS ON THE KINEMATICS AND FAULT-PLANE SOLUTION OF THE QUICHES FAULT ZONE REACTIVATED DURING THE 10 NOVEMBER 1946 ANCASH EARTHQUAKE, NORTHERN PERU

By Olivier Bellier, Jean François Dumont, Michel Sébrier, and Jacques Louis Mercier

Abstract

The Ancash earthquake of 10 November 1946 (M_w = 6.8) produced surface faulting along the Quiches normal-slip fault. Field studies reported discontinuous NW–SE to NNW–SSE-striking seismic scarps that displace Quaternary glacial moraines and outwash, as well as Mesozoic sedimentary rocks. Structural analyses show that the 1946 normal displacement was accompanied by a small left-lateral slip component. Morphological analysis of the fault scarp and observations in a trench excavated across the scarp show evidence of a single normal-fault displacement before the 1946 seismic event that offset late Pleistocene glacial moraines. This indicates an approximate recurrence interval of more than 13,000 ± 1,000 years for the major events, suggesting a rate of net vertical displacement on the fault of less than 0.25 mm/yr. Kinematic analysis along the Quiches fault, in comparison with other regional studies, suggests that the state of stress in the High Andes is regionally and locally homogeneous with only minor changes in the stress directions adjacent to major structures such as the Marañon Thrust and Fold Belt. The minimum horizontal stress ($\sigma 3$ axis) is oriented N10-25°E, the intermediate horizontal stress ($\sigma 2$ axis) is oriented N100-115°E, and the maximum stress ($\sigma 1$ axis) is vertical. We suggest that the 60°SW-dipping Quiches surface fault plane is connected at depth to a low-angle-dipping fault plane. This seismic fault is a reactivated thrust fault of the Tertiary Marañon Thrust and Fold Belt.

Introduction

Focal mechanisms of major earthquakes that occurred prior to establishment of the WWSSN in 1962 are commonly difficult to determine. In these cases, two approaches help to define a fault-plane solution: neotectonic analysis and seismological waveform modeling. The first approach, used in this study, is the kinematic and structural analysis of earthquake-related, tectonic surface faulting (see Mercier *et al.*, 1979, 1983; Philip and Meghraoui, 1983; Sébrier *et al.*, 1985, 1988; Cabrera *et al.*, 1987). Unfortunately, both seismologic and neotectonic methods are infrequently applied in the same region. Analysis of the Quiches normal fault, the source of the 10 November 1946 Ancash, Peru, earthquake (Figs. 1 and 2) offers the opportunity to examine an earthquake using both neotectonic field study and seismological analysis.

Field studies, performed some weeks after the 1946 Ancash earthquake (Silgado, 1951), reported NW–SE-striking, discontinuous, normal fault scarps, located on the Quiches heights, west of the steep Marañon River canyon. Later, Hodgson and Bremner (1953) proposed a strike-slip reverse focal mechanism for

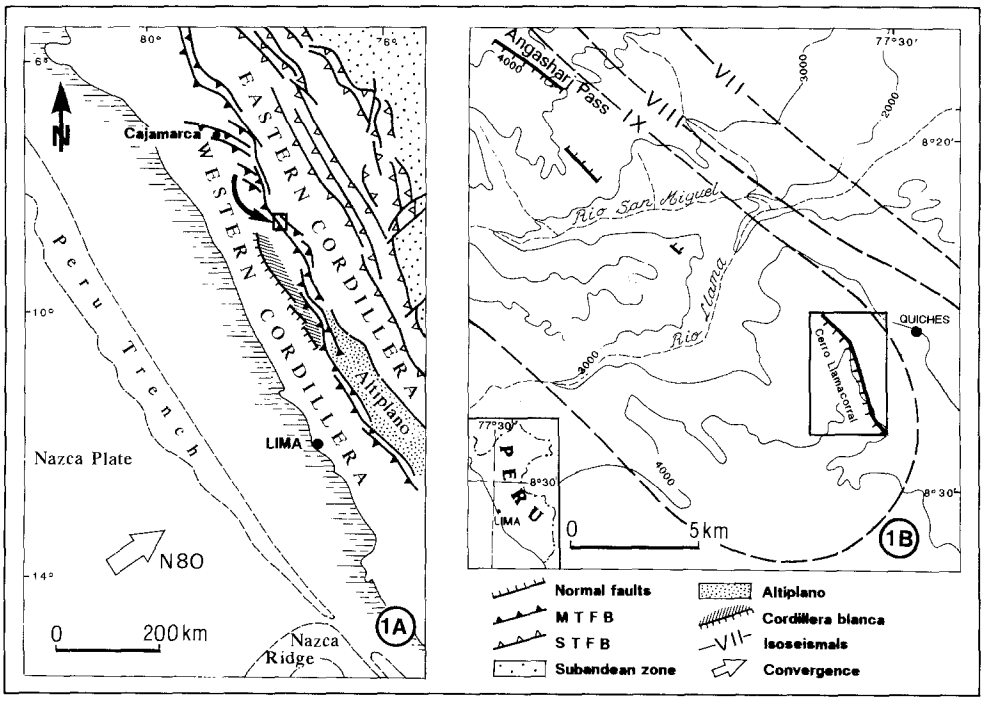


FIG. 1. (a)Regional geologic setting of the Quiches fault. "Convergence" is the Nazca plate convergence direction from Pilger (1984). MTFB is the Marañon Thrust and Fold Belt, and STFB is the Subandean Thrust and Fold Belt. (b) Map of the Quiches fault reactivated in 1946 (hatchured on the downthrown block). Dashed lines with roman numbers are the 1946 isoseismals (Silgado, 1951).

this earthquake and concluded that the normal surface faulting could be a secondary effect. But, from the same seismicity data, Suárez *et al.* (1983) proposed a normal fault-plane solution that agreed with the Silgado's surface observations, yet this solution is very poorly constrained. More recently, Doser (1987), using re-evaluated first-motion data and waveform modeling, computed two normal focal mechanisms that define a N135°E to N105°E-striking and 30°SW-dipping fault plane. Detailed mapping, morphological, and structural analysis and observations in a trench excavated across the fault scarp permit us (1) to establish the kinematics of the Quiches fault during the 1946 Ancash earthquake, (2) to recognize one major Pleistocene event prior to the 1946 earthquake, and (3) to compare our surface measurement of the slip-vector of the 1946 Quiches earthquake to the seismologically determined slip-vector previously reported by Doser (1987). Our results in conjunction with other field studies in the region (Sébrier *et al.*, 1985, 1988; Cabrera *et al.*, 1987; Bellier, 1989; Bellier *et al.*, 1989a) are finally the basis for characterizing the regional state of stress in the High Andes of northern and central Peru.

THE 1946 ANCASH EARTHQUAKE

The 10 November 1946 Ancash earthquake occurred at 17:43 GMT and was felt in an area exceeding 450,000 square km (Silgado, 1951, 1978). It caused about 1400 deaths, which is very high for such a sparsely populated region. Most destruction was caused by landslides; one slide had an estimated volume

of 25 million m^3. Silgado's intensity study (1951) shows that the isoseismal IX (on the Modificated Mercalli (MM) scale) bounded an elliptical area of 1600 square km. Maximum intensities of X MM were reported within this area where NW–SE surface ruptures were observed (Fig. 1). These ruptures located in the high Puna plateau, west of the demolished city of Quiches, were noted by Richter (1958) as the first well-observed example of major surface faulting produced by a strong earthquake in South America. An initial analysis of instrumental data (Silgado, 1951) located the epicenter at 8°20′S and 77°50′W and the focus at a depth of 30 to 40 km with a magnitude of $7^{1/4}$ (M_L). Recently, Doser (1987) re-evaluated first-motion data and concluded that the epicenter was located at 8°28.4′S-77°51.6′W, the focal depth was 15 to 17 km deep, and the magnitudes were 6.3 to 6.5 (M_s), 6.5 to 6.9 (m_b), and 6.8 (M_w).

The Peruvian catalog of historical seismicity (Silgado, 1978) reported no shallow earthquakes in the Quiches region between 1513 and 1946. Since 1946, Silgado (1947, 1948, 1949, 1957, 1978) reported relatively low seismicity in the Quiches region; the strongest event was recorded on 5 May 1971 with a magnitude of 4.9 (M_s). Also, a microearthquake study during October–November 1985 in the Cordillera Blanca area (Fig. 1) recorded six earthquakes of magnitudes 2.3 to 3.7 (M_L) with epicenters located in the Quiches area (Deverchère, 1988; Deverchère *et al.*, 1989).

The 1946 Quiches Fault Zone

The Quiches fault is situated in the northern part of the Ancash region, at an elevation of 3600 to 4100 m (Fig. 1 and 2). This fault is within the NW–SE-striking Marañon Thrust and Fold Belt (Fig. 1) of Tertiary age, which forms the northeastern part of the Western Cordillera. Within the thrust and fold belt, Cretaceous carbonate rocks have been thrust northeastward over the pre-Andean basement of the Eastern Cordillera (Heim, 1949; Wilson *et al.*, 1967; Mégard, 1984).

The 1946 earthquake produced about 21 km of discontinuous NW–SE-striking surface breaks (Heim, 1949; Silgado, 1951; Richter, 1958; Sébrier *et al.*, 1982, 1988) (Fig. 1). The main 1946 fault break is defined by two NW–SE to NNW–SSE-striking, SW-facing breaks that displace late Quaternary glacial and outwash deposits, as well as Mesozoic limestones and sandstones. The southernmost part of the 1946 rupture is termed the Llamacorral segment, and the northernmost part, the Angasharj segment (Figs. 1 and 2). The Angasharj segment is more than 3 km long and strikes between N55°-75°W. Its fault-plane dips 70°SW, and the maximum vertical down-throw on the fault (i.e., dip-slip component) is 1.25 m in Mesozoic quartzose sandstones (Fig. 3). The Llamacorral segment (Figs. 1, 2, and 4) is 4 km to the west of Quiches and has a 4-km-long scarp that strikes N20°W along the southern part and a 1.5-km-long scarp that strikes N50°W along its northern part. Quaternary glacial moraines (Fig. 5) and outwash deposits are displaced along the southern part of the Llamacorral segment and Cretaceous limestones are displaced along the northern part of it (Fig. 6). The limestones are vertically displaced up to 3.5 m (i.e., dip-slip component), and the glacial deposits are displaced up to 1.5 m by the 1946 earthquake (Fig. 3). The surface dips of the fault range between 49° and 78°SW with a 60°SW mean value. Antithetic and synthetic breaks 10 to 40 cm high are parallel to the main fault scarp. These breaks offset the modern soils and are situated where the major fault segment is complex and characterized by

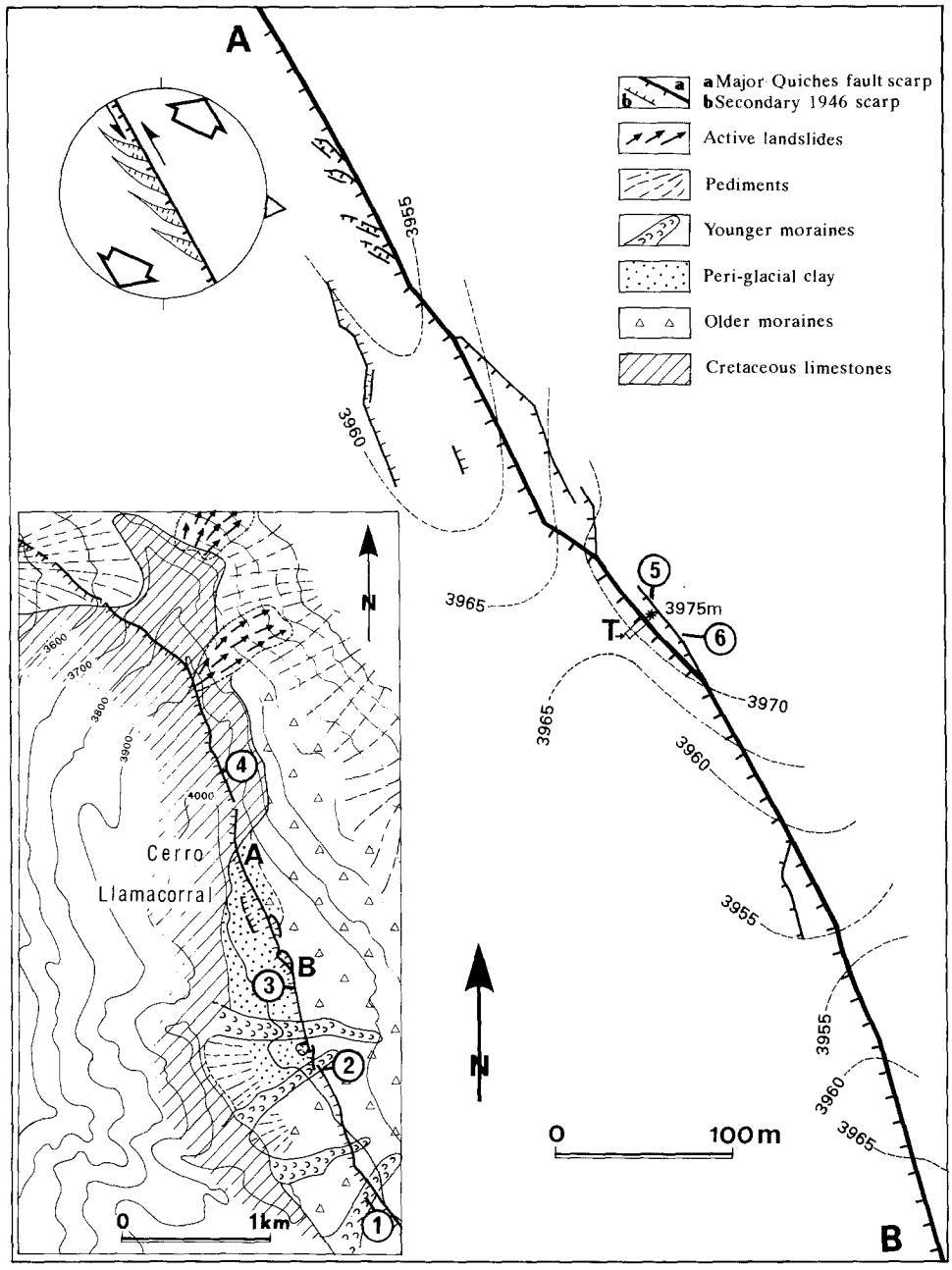


FIG. 2. (*Inset at bottom left*) Detail map of Llamacorral segment of the Quiches fault (hatchured on the downthrown block). Circled numbers 1 to 4: topographic profiles. (*Central part*) Detailed map of the A-B part of Llamacorral fault segment and location of the trench (T) and of the topographic profiles (circled numbers 5 and 6). (*In the circle at top left*) "En echelon" opened gashes set at the base of the 1946 scarps indicates the minor left-lateral slip component of the normal faulting.

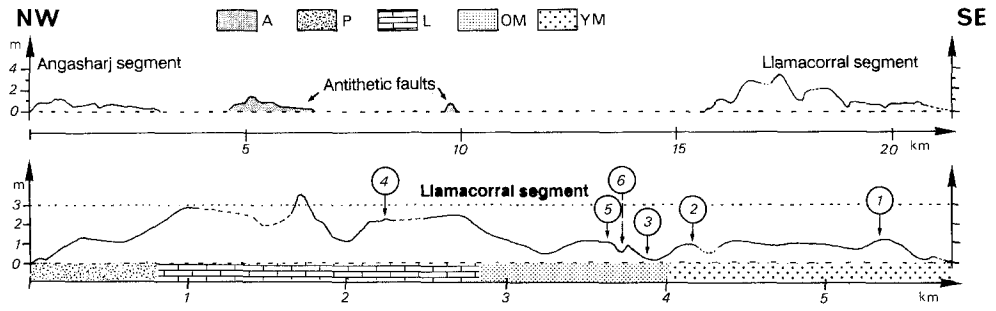


FIG. 3. (a)Distribution of the net vertical displacement produced by the 1946 Quiches earthquake versus distance along the fault strike. (b) Detailed profile showing the distribution of the net vertical displacement along the Llamacorral segment fault strike. Arrows point to the location of the morphological scarp profiles numbered in the circles and shown in Figure 7. Lithology of offset rocks: P: pediments and colluvium; L: limestones; OM: "older moraines"; YM: "younger moraines."

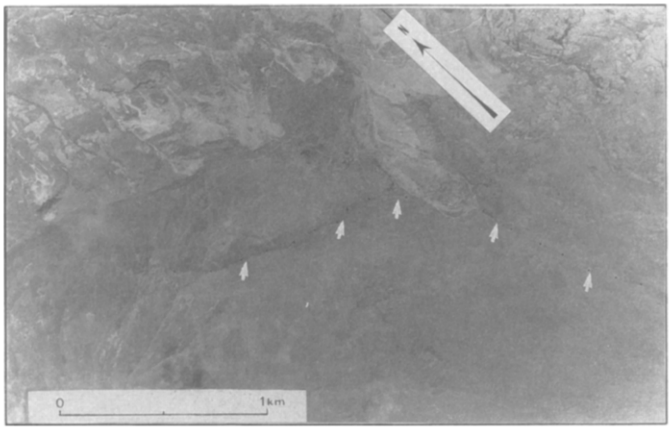


FIG. 4. Aerial view showing the Northern part of the Llamacorral fault segment. Arrows underline the 1946 fault scarp.

bends or splays (Figs. 2a and b; Fig. 7, profiles 5 and 6). The Llamacorral and Angasharj segments are separated by a 12-km-long gap in surface ruptures. In addition, two average 58°NE-dipping antithetic surface faults are 3 km to the SW, parallel to the main fault with approximate lengths of 0.4 and 2 km (Fig. 1), the longest one having a maximum vertical displacement of 1.7 m in Cretaceous limestones (Fig. 3). The individual lengths of all four rupture segments total to just 10.9 km.

All of the 1946 scarps in the Quiches area show a normal faulting sense of displacement. Moreover, the earthquake produced extensional tectonic deformation such as open fissures and small grabens at the base of the fault scarps (Fig. 7, profiles 1 and 2). Clear examples of active tectonic geomorphology are present along the southern part of the Llamacorral fault segment (Fig. 2), where four Holocene moraine crests are displaced. The two glacial valley floors, which are located between these moraine crests, are displaced forming a sagpond on the downthrown block of the northern glacial valley.

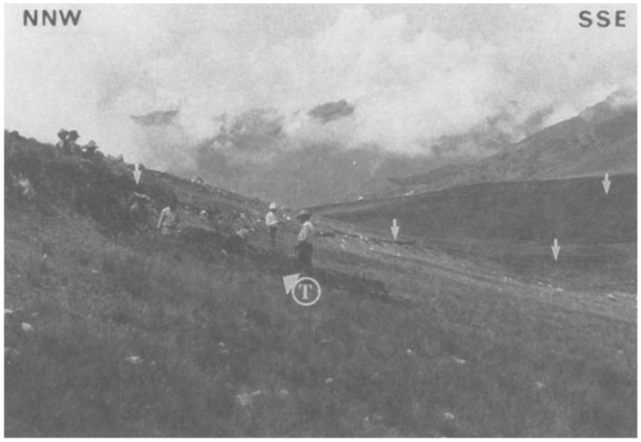


FIG. 5. Photograph of the Llamacorral fault scarp affecting the older moraines nearby the Trench (T; see location on Fig. 2). Arrows point to the 1946 fault scarp.

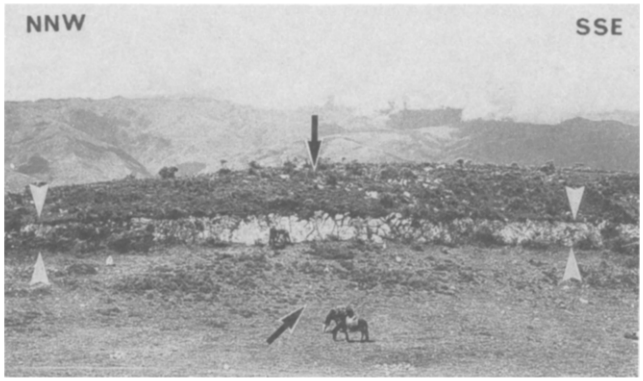


FIG. 6. View to the northeast, of the Llamacorral scarp on Cretaceous limestones. White arrows point to the 1946 scarp; black arrows point to slope-break that define the pre-1946 scarp. The low slope-angle of the pre-1946 scarp is suggestion of relatively long recurrence intervals for the Quiches fault.

THE STRATIGRAPHY OF QUICHES FAULTED MORAINES

The fault in the Llamacorral segment displaces two morainal deposits that have a heavy cover of grass, as has the rest of the terrain. Characteristics of these allow us to distinguish two generations termed "the younger moraines" and "the older moraines" (4 and 2 on Fig. 2). The moraine characteristics allow us to make a tentative correlation between these Quiches moraines and moraines at other Peruvian localities.

The *younger moraines* are represented by four well preserved moraine crests that bound two glacial valleys (Fig. 2). The summits of the moraine crests are covered by a thin horizon of peaty soils. The till components are very poorly weathered. The limestone boulders and clasts are very fresh but lichen covered, and the moraines are poorly consolidated. These younger moraines are not of Late Holocene age because the Late Holocene moraines in Peru are represented by fresh lateral and terminal moraines that are almost completely unvegetated

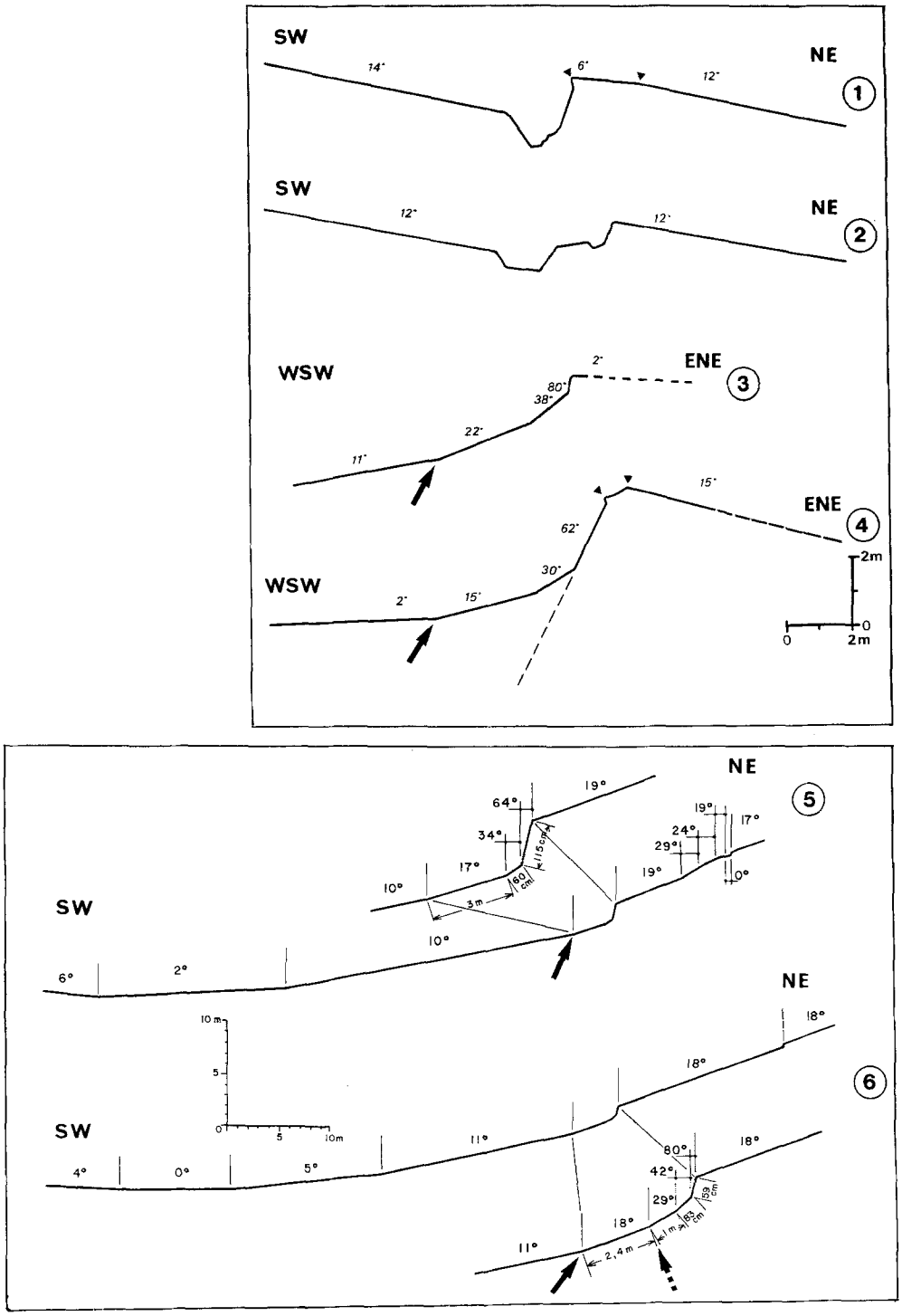


FIG. 7. Topographic profiles across the Llamacorral fault scarp (see circled numbers on Figs. 2 and 3 for location). Profiles 1 and 2 are situated along two younger moraine crests; profile 4 in Cretaceous limestones; profiles 3, 5, and 6 in older moraines. Black arrows point to the slope-break that define the toe of the pre-1946 scarp. F is the fault plane.

(e.g., Mercer and Palacios, 1977; Wright, 1984). However, the good preservation of the glacial landforms and the very low degree of diagenesis of the younger moraines leads us to tentatively assign this glacial landform to the advance of the last glaciation (i.e., Late Wisconsinian of North America). Indeed, these Quiches younger moraines share strong geomorphic and weathering similarities with the moraines of the last glacial readvance of the last glaciation that are exposed in the Cordillera Blanca approximately 100 km SW of Quiches. This Cordillera Blanca glacial event yielded radiocarbon dates ranging between 11,000 to 14,000 yr B.P. (Clapperton, 1981), which is also in agreement with ages of dated moraines from other localities in Peru that present characteristics similar to those of the Quiches moraines. In the Junín area of the central Peruvian Andes, a similar sequence of the last glaciation culminated at about 12,000 year B.P. (Hansen *et al.*, 1984; Wright, 1984). In Southern Peru around the Cordillera Vilcanota, the last glaciation culminated between 28,000 and 14,000 yr B.P. with a major readvance at 14,000 yr B.P. (Mercer and Palacios, 1977; Mercer, 1983). More recently, radiocarbon datings from morainal samples located in the western part of the Eastern Cordillera, 80 km north of Quiches, confirm that the regional deglaciation of the Peruvian Andes was underway by about 12,000 yr B.P. and the major readvance was about 14,000 yr B.P. (Birkeland *et al.*, 1989).

The *older moraines* are characterized by a lake of glacial landforms and weathered till deposits. These moraines are only observed on the fault breaks and in valley sections. They are covered by a well developed peaty soil. The limestone boulders and clasts are deeply rilled by solution and covered by lichen; the till is very well consolidated and shows a high degree of diagenesis. We speculate that these moraines were deposited during an early stage of the last glaciation more than 42,000 yr B.P. (Wright, 1984).

Hence, based on the above observations, we estimate an age of 13,000 ± 1,000 yr B.P. for the younger moraines and of at least 42,000 yr B.P. for the older moraines.

Multiple Displacements and Paleoseismicity

Fault Scarp Morphology

Scarp morphology can be used to estimate the age of fault scarps. These methods, which were developed for Quaternary fault scarps in the western United States (e.g., Wallace, 1977, 1984; Bucknam and Anderson, 1979; Nash, 1980; Hanks *et al.*, 1984), have been applied in the Peruvian Cordillera (Cabrera *et al.*, 1987; Cabrera, 1988; Schwartz, 1988; Bellier, 1989; Bellier *et al.*, 1989a), where semi-arid climatic conditions are similar to those prevailing in the western United States. We have measured numerous profiles across fault scarps using methods documented by Wallace (1977) and analyzed the relationships between scarp height, slope angle, and probable age. To evaluate the ages of the Quiches fault scarp, we have compared the Quiches scarp profiles with the western United States dated fault scarp profiles (e.g., Wallace, 1977).

Where the 1946 break crosses the younger moraine crests, its morphology is consistent with a Holocene single event scarp (Figs. 2 and 3, and Fig. 7, profiles 1 and 2). Here, the scarp slope is in an opposite direction to the moraine crest slope. The west-facing steep scarp and associated grabens at the toe of the scarps, abruptly break off the gently east-dipping slope of the moraine crests. The west-facing scarp (profile 1) shows a regular dipping slope, indicating that

only the 1946 event has faulted the younger moraines. Hence, it might be inferred that the 1946 rupture produced the destruction of older scarps. However, local elderly inhabitants who know perfectly the 1946 breaks in the Quiches area reported to us that these breaks did not exist before the 1946 earthquake. The profile 2 exposed a more complex scarp associated with two grabens, but its morphology also characterized a single event scarp. Thus, the last surface faulting on the Quiches fault, prior to the 1946 event, is older than the younger moraines, i.e., older than 13,000 ± 1,000 years.

The four other topographic profiles are from the breaks that affect the limestones and the older moraines (Figs. 2 and 3, and Fig. 7, profiles 3, 4, 5, and 6). Profile 4, situated in the Cretaceous limestone (Fig. 6), exhibits a sharp break in slope at the crest of the scarp, a steep free face of average 2 m and maximum 3.5 m high, with a dip of 60° to 70°, and a small debris slope at the scarp toe. These small debris slope have dips of 38°, 30°, 34°, and 42° for the profiles 3, 4, 5, and 6, respectively (see values of the angles just above the arrows). We interpret the 29°-dipping slope on profile 6 as the lower part of the debris slope, i.e., as a well expressed wash slope. Profiles 3, 5, and 6, situated in the older moraines (Fig. 5), also exhibit a sharp break in slope at the crest, a free face more than 1 m high with a dip of 60° to 80°, and a small debris slope. These morphological characteristics are evidence for a simple, single-event scarp resulting from the 1946 rupture. However, a detailed topographical profile analysis in the limestones (profile 4) and in the older moraines (profiles 3, 5, and 6), shows a slight slope break, at 3 to 4 m to the west of the 1946 main scarp (marked by arrows on Fig. 6 and Fig. 7, profiles 3, 4, 5, and 6), which agrees with Schwartz's (1988) observations. On a photograph from Silgado (1951), Schwartz noted a break in slope that defines a pre-1946 scarp and suggested that the low slope angle belongs to an older scarp, thus indicating significantly long recurrence intervals for the fault activity. According to Wallace's studies in the western United States (1977), this low (between 15° and 22°) dipping slope scarp angle should correspond to ages older than 12,000 yr. This is in agreement with the data provided by profiles 1 and 2 measured on the younger moraines, which do not exhibit this low slope angle.

The small facet above the fault crest (delimited by triangles) and the lower debris-slope (30°) in profile 4 (Fig. 7), as well as the faceted upper surface (6°) in profile 1, would also indicate that both are compound scarps. However, the scarp morphology in profiles 1, 2, 3, and 4 are complicated because the dip of the far-field slope is in a opposite direction to the scarp face. In addition, the small ledge at the top of the free face in profiles 1 and 4 (delimited by triangles in Fig. 7) probably results from a loose cohesion of the surficial cover that overlies the faulted bedrock.

In conclusion, we interpret only the low slope angle (above the thick arrows on profiles, 3, 4, 5, and 6) as convincing of a compound scarp, which represents the penultimate rupture on this segment and indicates a very long recurrence interval (> 12,000 yr) for major seismic events. That the rate of scarp degradation is faster than the rate of present-day scarp formation is our explanation of the nearly monogenetic aspect of the fault scarp morphology.

Trench Observations

Colluvial wedges and paleosols adjacent to the fault plane in trenches are commonly used as evidence for the number of past surface faulting events along

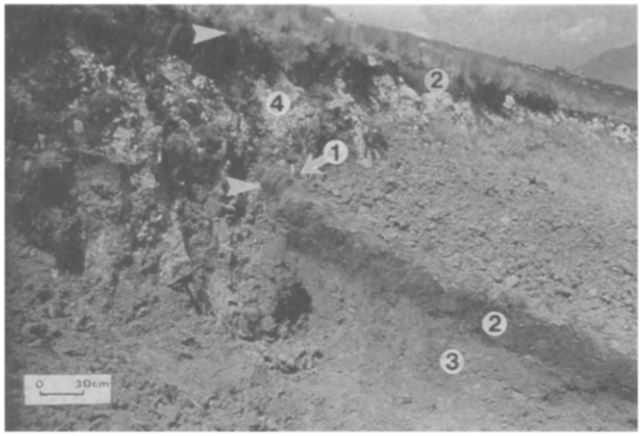


FIG. 8. Photograph of a section of the trench excavated across the Quiches fault (location T, on Fig. 2). (1) 1946-scarp debris-slope deposit, (2) present-day peaty brown soil, (3) brownish-orange clay deposit of the downthrown block interpreted as an older colluvium, and (4) the older moraines. White arrows point to the 1946 fault scarp.

a given scarp (Swan *et al.*, 1980; Schwartz and Coppersmith, 1984; Sieh and Jahns, 1984; Cabrera *et al.*, 1987; Meghraoui *et al.*, 1988; Schwartz, 1988). Therefore, we excavated a trench in order to perform more detailed observations within the colluvial wedge and on the seismic fault plane. Several factors led us to excavate only one trench. First, it was difficult to dig trenches within the limestone and sandstone. Second, where the 1946 fault scarp affects moraines, the base of the scarp is frequently characterized by open fissures and small graben along the fault. Therefore, the lack of friction near the surface does retain evidence (e.g., slickensides) of the 1946 slip vector on the fault plane. The only suitable site to excavate a trench for our purposes was roughly in the middle part of the Llamacorral segment, where the fault scarp crosses moraines without exhibiting fissures (Fig. 2).

In the trench, there is no evidence of interbedded colluvial wedges or paleosols on the downthrown block (Figs. 8 and 9) indicating that the Quiches scarps are Holocene single-event scarps. The upthrown block (log A on Fig. 9) exhibits the present-day peaty brown soil (2) above well indurated old moraines (4). Adjacent to the main fault plane, the downthrown block (log B on Fig. 9) has a very small debris slope (1) from the 1946 earthquake that overlies the present-day peaty brown soil and is forming the modern colluvial wedge. The soil is developed on a homogeneous brownish-orange clay deposit (3). Rare weathered carbonate gravel-debris are dispersed within the clay. This deposit is interpreted as a old weathered colluvial wedge that resulted from the degradation of a scarp that formed during to a Late Pleistocene event; i.e., older than 13,000 ± 1,000 yr B.P.

Within the trench, the peaty soil (2 on Fig. 9) is clearly offset by the 1946 seismic event, which produced 1.4 m of vertical throw at this locality. The trench bottom, which is more than 2 m deep, has not reached the glacial deposits. Thus, restoring the state prior to the 1946 offset, the trench profile (Fig. 9) shows that the older moraines had been previously affected by at least one older normal offset that had produced a scarp more than 2 m high, i.e., more than the depth of the excavation. The degradation of this ancient scarp

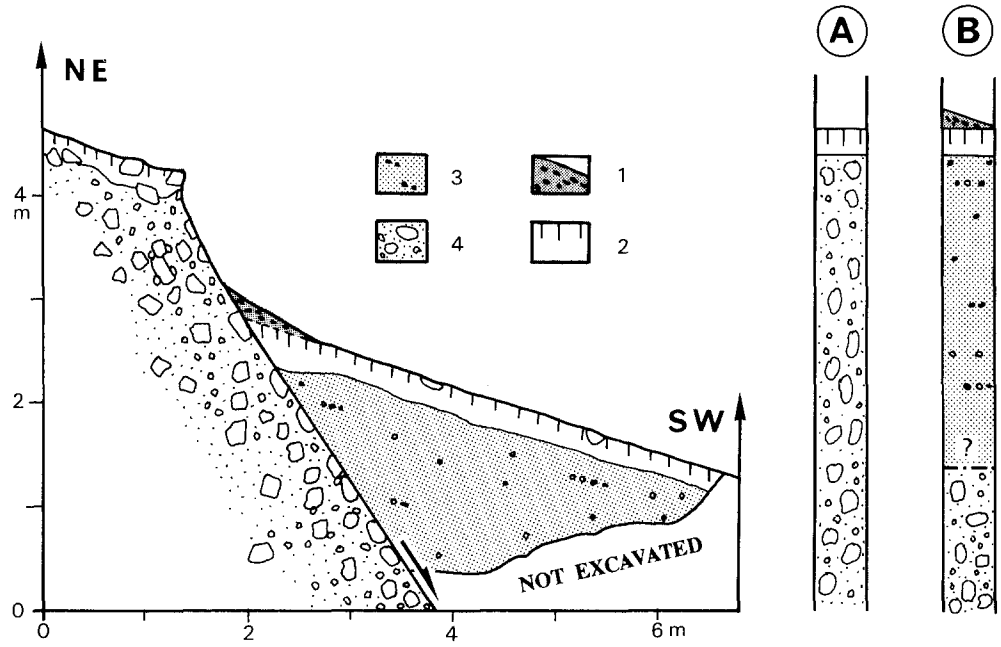


FIG. 9. Sketch of the trench. A and B represent the deposit logs of the upthrown block and of the downthrown block, respectively. Same symbols as on Figure 8.

has produced accumulation of a colluvium wedge on the downthrown block. This colluvium has been weathered to the present-day brownish-orange clay. Relationships in the trench and the preponderance of compound scarp morphologies are convincing evidence for more than one slip event. Thus, both stratigraphic relations and our interpretation of the scarp morphology are in agreement with only one normal displacement event (i.e., 1946) on the Quiches fault during the past 13,000 ± 1,000 years. Yet, as there is no evidence of paleosols interbedded within the 2-m-thick older colluvium, the greater than 2 m offset affecting the older moraines probably corresponds to a single Late Pleistocene seismic event. This slip event, penultimate to the 1946 earthquake, predates the younger moraines and postdates the older moraines.

Paleoseismicity of the Quiches Fault

According to our age estimation of the Quiches moraines, the Late Pleistocene slip event (i.e., pre-1946) that occurred prior to the main readvance of the last glaciation should be older than 13,000 ± 1,000 yr B.P. If we consider that the interval between this event and the 1946 earthquake is representative of the Quiches fault recurrence, we can estimate that the recurrence interval for major seismic events is greater than about 13,000 ± 1,000 years. This recurrence interval is much longer than those for the Cordillera Blanca fault zone affecting the Western Cordillera 100 km east of Quiches (Fig. 1), which were estimated in the order of 3000 years (Bonnot, 1984; Bonnot *et al.*, 1988) or 2440 ± 1060 years (Schwartz, 1988).

An approximate mean rate of vertical movement can be inferred from these data. The maximum and minimum net vertical displacement for the 1946 event

are given by the 3.5-m- and the 1.5-m-high scarps that are seen in the northern part of the Llamacorral fault segment and within the Mesozoic limestones and the moraines, respectively. Assuming that the strain producing these 3.5 m or 1.5 m vertical displacements accumulated over 13,000 ± 1,000 years, the approximate mean rates of vertical movement should range between 0.27 ± 0.02 and 0.11 ± 0.01 mm/yr. Taking into account that these rates are maximum estimates, they indicate that the vertical slip rate of the Quiches fault is much less than the vertical slip rate of 0.7 mm/yr (Bonnot, 1984; Bonnot *et al.*, 1988) or 0.86 to 1.36 mm/yr (Schwartz, 1988) on the Cordillera Blanca fault zone. On the other hand, the rate of the Quiches scarp degradation is faster than the vertical slip rate on the Quiches fault.

Kinematics of the Quiches Fault

Field observations along the Quiches fault scarps show that the main component of the 1946 surficial displacements was normal (Heim, 1949; Silgado, 1951; Sébrier *et al.*, 1982, 1988). Observations of en-echelon open gashes, striking N50-60°W, oblique to the main fault also indicate a small left-lateral strike-slip component (Fig. 2). Examination of striations on the major fault plane observed in the trench confirm that the left-lateral strike-slip component of motion for the 1946 event. We also document evidence of a complex tectonic history that predates the 1946 earthquake using striations.

Quiches Fault Kinematic History

The major fault plane affecting the Cretaceous limestones is very polished and exhibits three successive directions of slip, evidenced by three superimposed families of striations (Fig. 10). The oldest slip (1) is represented by stylolitic striations (Sébrier *et al.*, 1982, 1988). The penetrative oblique-stylolite column-ends (e.g., Mattauer, 1973; Hancock, 1985) indicate the reverse movement of this slip. This first slip predate right-lateral strike-slip stylolitic striations (2). These stylolitic striations (1 and 2), which affect the limestones, were formed by a pressure-solution mechanism (i.e., by creep within diffusion mechanism) at a

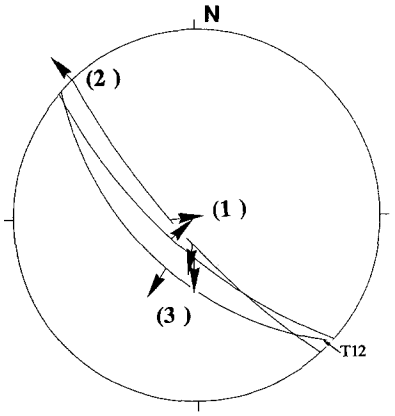


FIG. 10. Chronology of the three successive slip directions measured on the Quiches major fault and resulting from three successive Neogene to Quaternary stress regimes. Arrows attached to fault traces correspond to the measured striation "s" (Wulff stereonet, lower hemisphere). The numbers in brackets give the chronology between the three successive directions of slip, evidenced by three generations of striations. T12 indicates the major fault plane affecting the older moraine, and the other fault planes are measured in Cretaceous limestones.

depth ranging between about 1 and 4 km. They predate normal striations (3), corresponding to a frictional dip-slip (i.e., purely brittle fault deformation), which indicates a normal movement with a small left-lateral strike-slip component (Fig. 10). Grooves and frictional striations corresponding to normal slip (3) are imprinted on the fault planes affecting moraines. Within the trench we observed, on the major fault plane, parallel rough grooves and thin frictional striations on slickensides that affect both the morainal pebbles and matrix. Thus, these near surface striations were produced by both the Late Pleistocene and the 1946 earthquake slip events (Fig. 10). These three successive slip directions (1, 2, and 3) are interpreted to result from three successive stress regimes.

Finally, the successive Quiches fault slip orientations (1, 2, and 3) demonstrate that the 1946 earthquake produced displacement on an inherited fault plane. Indeed, this seismic normal faulting has reactivated a reverse fault of the Marañon Thrust and Fold Belt. The reverse faulting was imprinted by the reverse stylolitic striations in agreement with an E–W to NE–SW trending shortening which characterized late Eocene and Neogene thrust and reverse fault kinematics of the Marañon Thrust and Fold Belt (e.g., Mégard, 1984; Bellier *et al.*, 1989b; Sébrier *et al.*, 1982; Sébrier and Soler, 1990). Thus, the Quaternary and 1946 normal slips have reactivated a Tertiary reverse fault of the Marañon Thrust and Fold Belt.

Slip Vectors of the 1946 Quiches Seismic Shock

Striations on the major seismic fault plane have been observed on outcrops of Mesozoic limestones (C07, C08, C16, Fig. 11c and d) and of Late Pleistocene moraines (M01 at 06). Within the trench excavated across the older moraines, we observed both striations on the major fault plane (T12) and striations on minor fault planes (T9, T10, T11, T13, T14, T15). Fault kinematic analysis was first conducted using a graphical method (Vergely *et al.*, 1987). The measured major seismic fault planes have strikes ranging between N125° and N190°, with dips between 49° and 78°SW; all their slip-vectors show nearly dip slips that correspond to normal movements with a small left-lateral slip component as pitches range between 69° and 87°S. Similarly, the minor fault planes, striking between N–S and NW–SE, generally show the same resolved slip vectors as the major one. An exception is the nearly E–W-striking and S-dipping fault plane (T10, Fig. 11 d), which shows a normal striation with a minor right-lateral slip component. Thus, orientations of these striations trend between N–S and E–W, depending on the strike of the plane on which the striations lay, and so are in agreement with a roughly N–S to NE–SW-trending extension.

To determine the state of stress that produced the 1946 Quiches earthquake (Fig. 11c), we used the quantitative method proposed by Carey (1979). Our analysis of the slip vectors in terms of stress assumes that the sliding shown by the striations occurs in the direction of the shear stress resolved on each preexisting fracture. Conversely, a mean deviatoric stress tensor may be computed from a set of striated faults, which best explains the observed striations (Carey, 1979; Carey and Brunier, 1974). Carey's inverse method minimizes the deviation between the calculated slip vector (**t**) and the observed striation (s). Inversion of the data gives the azimuths and dips of the principal stress axes ($\sigma 1, \sigma 2, \sigma 3$) of the deviatoric tensor and the "stress ratio" $R = (\sigma'2 - \sigma'1)/(\sigma'3$

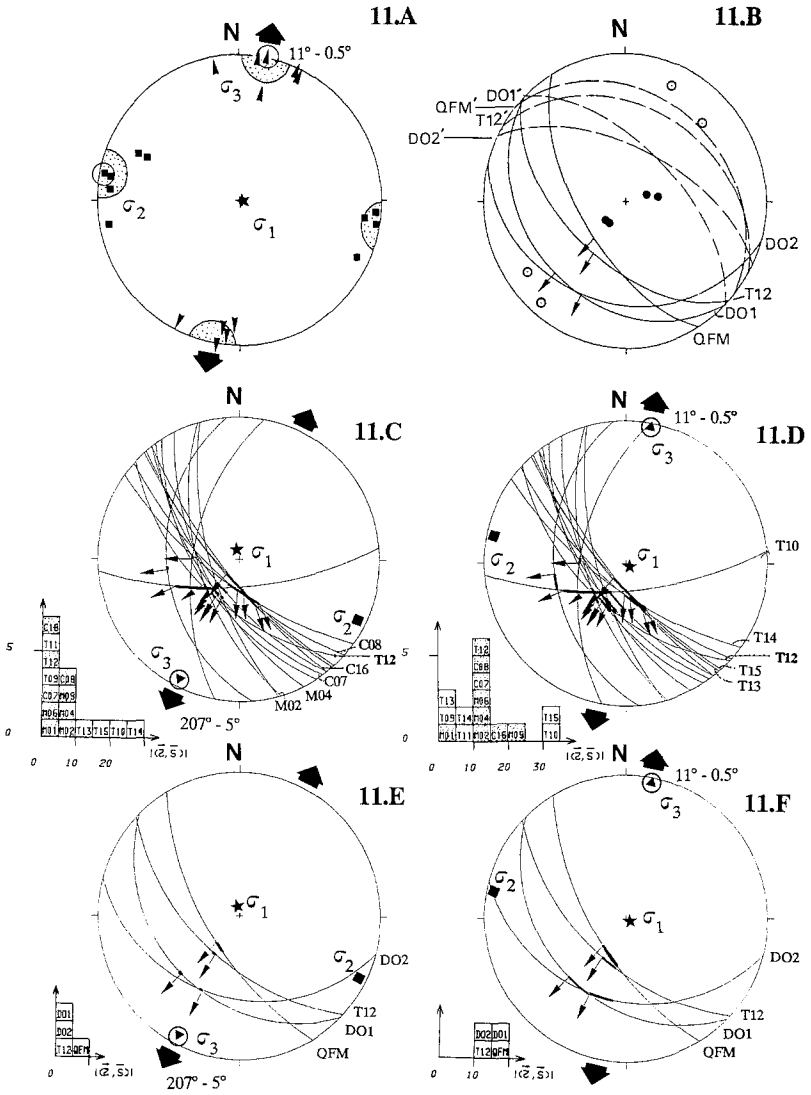


FIG. 11. (a)Regional stress directions computed by the Fisher statistic method on 10 stress tensors computed from Quaternary and Holocene normal faults of the High Andes (see Table 1). The triangles represent the $\sigma 3$ axes and the squares the $\sigma 2$ axes analyzed by the Fisher statistic method. Divergent large black arrows give azimuths of $\sigma 3$ axis. Dotted areas show the Fisher cone dispersion (95 per cent reliability), circled triangle and square show the mean $\sigma 3$ and $\sigma 2$ axes, respectively. (b) Focal mechanisms of the 9 November 1946 Ancash earthquake (Schmidt stereonet projection, lower hemisphere). QFM and T12 represent focal mechanisms deduced from the structural field study: (QFM) is the focal mechanism that we have determined computing an average main striated fault plane and (T12) is deduced from the main Quiches fault plane measured in the trench. DO1 and DO2 are Doser's focal mechanisms calculated by re-interpretation of the first-motion data (DO1) and by waveform modeling (DO2). Solid lines are the active nodal fault planes (QFM, T12, DO1, DO2); arrows represent the slip-vectors on fault-planes; open circles the T axes, and black circles the P axes. (c) Active normal fault data measured along the Quiches fault and used to compute the solution (see QU, Table 1). Numbers outside stereonets refer to data inside the histograms. Arrows attached to fault trace correspond to the measured slip-vector "s" (Wulff stereonet, lower hemisphere). Thick line segment on fault traces and histograms shows deviations between measured s and predicted t slip vectors for each fault plane. Divergent large black arrows give azimuth of the minimum $\sigma 3$ computed principal stress direction. Dotted areas on histograms indicate the major Quiches fault measurements. (d) Quiches active faults population tested with the regional stress tensor computed by Fisher statistic method (see Table 1 and Fig. 11a). (e) and (f) Fault planes of focal mechanisms, related to the 10 November 1946 earthquake, deduced from our field study (T12, QFM) and from Doser's seismic study (DO1, DO2) and tested with the computed local stress tensor (Fig. 11e) and the regional stress tensor (Fig. 11f) (projection Wulff, lower hemisphere).

TABLE 1

PARAMETERS OF THE DEVIATORIC STRESS TENSORS COMPUTED FROM THE QUARTERNARY AND HOLOCENE NORMAL FAULTS OF THE HIGH ANDES OF NORTHERN AND CENTRAL PERU

				Principal Stress Directions						
				$\sigma 3$		$\sigma 2$		$\sigma 1$		
Site	D	Latitude S	Longitude W	Azimuth	Dip	Azimuth	Dip	Azimuth	Dip	R
CH	H	07°41′	77°59′	007°	2°	097°	7°	264°	83°	0.64
QU	H	08°24′	77°31′	207°	5°	116°	5°	343°	83°	0.61
CU1	H	13°30′	71°56′	188°	7°	097°	7°	324°	80°	0.42
CU2	H	13°30′	72°00′	185°	4°	095°	2°	345°	85°	0.69
CB1	H	09°27′	77°30′	183°	9°	274°	5°	033°	80°	0.55
CB2	P	09°38′	77°28′	190°	1°	100°	1°	294°	89°	0.70
CB3	H	10°00′	77°15′	350°	5°	259°	4°	131°	84°	0.69
AY1	P	13°05′	74°10′	026°	4°	294°	19°	128°	70°	0.54
AY2	P	13°03′	74°08′	024°	3°	293°	15°	124°	74°	0.35
AY3	P	13°07′	74°12′	012°	19°	280°	5°	175°	71°	0.59
Regional Stress Tensor				011 ± 10°/0.5°		281 ± 10°/2°		113 ± 10°/87°		0.58 ± 0.09

Sites: CH: Chaquilbamba active fault (Bellier, 1989; Bellier *et al.*, 1989a); QU: Quiches fault (this study; see data on stereonet 11c, Fig. 11); CU1 (Sébrier *et al.*, 1985), CU2 (Cabrera *et al.*, 1987): Cuzco fault zone; CB1-CB2-CB3 and AY1-AY2-AY3 (Sébrier *et al.*, 1988) Cordillera Blanca active fault zone and Ayacucho basin Quaternary faults.

Azimuths are measured clockwise from north; dip is toward the measured azimuth.

$R = \sigma'2 - \sigma'1/\sigma'3 - \sigma'1$ is the "stress ratio" of the stress tensor.

D corresponds to the age of the normal faulted Formations; H: Holocene; P: Pleistocene. The regional stress tensor corresponds to the directions computed by Fisher statistic method; and $R = 0.58 \pm 0.09$ to the mean arithmetic value.

$- \sigma'1$). The R value varies between two extremes: 0 as $\sigma'2 = \sigma'1$ and 1 as $\sigma'2 = \sigma'3$. The result is considered reliable if 80 per cent of the angles (t, s) between the calculated slip vector (**t**) and the observed striation (s) are lower than 20° and if the computed solution is stable. The inversion of the above data gives a N207°-trending azimuth for the minimum (extensional) principal stress ($\sigma 3$) (Fig. 11c; Table 1: QU); the intermediate principal stress ($\sigma 2$) trends N116° and the maximum (compressional) principal stress ($\sigma 1$) is roughly vertical. Both $\sigma 3$ and $\sigma 2$ axes are roughly horizontal, and the stress ratio ($R = 0.61$) shows that the deviatoric $\sigma'2$ value is tensional but strongly different from the $\sigma'3$ one, and consequently the direction of extension ($\sigma 3$) is well constrained. These tensorial parameters indicate that the local state of stress is extensional with a NNE–SSW-trending tension.

Regional Extensional State of Stress in the High Andes

The previous result may be only significant on a local scale. Consequently, to determine the regional state of stress, we used the 10 stress tensors (Table 1; Fig. 11a) previously defined from field studies in the High Andes of central and northern Peru (see references in the Table 1 caption). These 10 stress tensors have minimum principal stress axes ($\sigma 3$) striking between N10°W (CB3) and N27°E (QU: this study) and maximum principal stress axes ($\sigma 1$) nearly vertical. The Fisher statistic method (modified by Watson, 1960) has been applied to compute the mean regional state of stress corresponding to these 10 tensors. It gives mean N11° ± 10°E-trending $\sigma 3$ and N281° ± 10°E-trending $\sigma 2$ axes (Fig. 11a; Table 1). The mean arithmetic value of the stress ratio R is 0.58 ± 0.09. In fact, if we only take into account the better constrained and

TABLE 2

FAULT-PLANE SOLUTIONS OF THE 1946 ANCASH EARTHQUAKE, PLOTTED ON STEREONET OF FIGURE 11b

	Nodal Planes		Slip Vector (Rakes)	*P* axis		*T* axis	
Number	Strike	Dip	Pitch	Azimuth	Dip	Azimuth	Dip
DO1	N135°E	30°S	90°W	N225°E	75°	N045°E	25°
DO1′	N135°E	60°N					
DO2	N105°E	30°S	80°W	N218°E	74°	N022°E	15°
DO2′	N116°E	60°N					
QFM	N149°E	63°W	82°S	N082°E	72°	N234°E	16°
QFM′	N130°E	28°N					
T12	N133°E	55°S	84°E	N074°E	78°	N220°E	10°
T12′	N120°E	36°N					

DO1-DO1′ and DO2-DO2′ represent fault-plane solutions (Doser, 1987) from first-motion data and from waveform modeling, respectively; QFM-QFM′ and T12-T12′ represent the fault-plane solutions deduced from field geological data.

more stable computed solutions (i.e., CH, QU, CU2, CB2, CB3, AY1, AY3 in Table 1), the stress ratio values is then 0.65. We chose this better constrained R value for the computed tests of the regional stress tensor on the Quiches fault planes.

This statistical mean regional extensional stress tensor has been used to compute predicted (t) slip vectors on the Quiches fault planes (Fig. 11d). The deviation (t, s) between the computed (t) and measured (s) slip vectors being small (see the histogram in Fig. 11d), this test clearly shows that the slip vectors on the Quiches fault are in agreement with the regional state of stress. Therefore, the 1946 seismic slip event on the Quiches fault is in agreement with the regional N11° ± 10°E-trending extensional direction which is near the N27°-trending extensional direction obtained locally around the Quiches fault.

Field Constraint on the Fault-Plane Solutions

Doser (1987) proposed two fault-plane solutions for the 1946 Ancash earthquake. One is based on re-evaluation of first-motion polarities. The best-fitting mechanism is the 30°SW dipping fault plane with an azimuth of 135° and a mean rake of 90°. This solution corresponds to a T axis that trends N45°E and dips at 25° and a P axis that trends N225°E and dips at 75° (DO1, Table 2; Fig. 11b). Nevertheless, this solution is poorly constrained because the rake may vary between −40° and −120°. It is roughly similar to the mechanism proposed by Silgado (1951) and Suarez *et al.* (1983), the only major difference being the low angle-dip of 30° instead of the 58° dip proposed by Silgado. The second focal mechanism has been computed by modeling long-period P waves of several seismograms; it is characterized by a N105° ± 20°-striking and 30° ± 10°SW-dipping fault plane, with a rake of −100° ± 10° (i.e., mean 80° ± 10°W pitch). This second solution has a T and P axes: N022°E/15° dip and N218°E/74° dip, respectively (DO2, Table 2; Fig. 11b). This can be resolved on the major fault plane, as a purely normal movement or a normal movement with a minor right-lateral strike-slip component (80° ± 10°W pitch).

To compare seismological and geological results, we have constructed the fault-plane solution corresponding to our field observations of striations. First,

the strike and dip of the Quiches major fault plane have been defined by a Fisher's statistic method (modified by Watson, 1960) applied on some 30 measurements of the major fault plane, then by the direct measurement of the major fault plane exposed within the trench. The Fisher's statistic method determines a mean fault plane striking 149°, dipping 63°SW, with a 82°SE slip-vector pitch (QFM on Fig. 11b; Table 2). The major fault plane measured within the trench strikes 133°, dips 55°SW with a 84°SE slip-vector pitch (T12, Table 2; Fig. 11b). These two major fault plane measurements display a normal movement with a minor left-lateral strike-slip component.

Fault-plane solutions given by the seismological and the geological field data are very similar (Fig. 11b). However, the active fault plane azimuth given by re-evaluating first-motion data (DO1) agrees better with the surface field observations than with one given by waveform modeling (DO2). Moreover, the latter plane is clearly oblique with respect to the regional direction of the Marañon Thrust and Fold Belt and is in discrepancy with the minor left-lateral slip component observed at the surface.

Focal Mechanisms, Regional State of Stress, Normal Fault Geometry, and the Moment Magnitude of the 1946 Earthquake

Focal Mechanisms and Regional State of Stress

The seismic slip vectors inferred from Doser's fault-plane solutions (DO1 and DO2 in Fig. 11b,e, and f) and from the main fault planes determined from this study (QFM and T12 in Fig. 11b, e, and f) have been tested using the local Quiches (Fig. 11c) and regional (Fig. 11a) stress tensors. The deviations between the slip vectors (**t**) computed with both the local and the regional stress tensors, and the seismic slip vectors (**s**) are small, showing that the latter agree with both the N11°E- and N27°E-trending extensions (Fig. 11e and f). However, the WNW–ESE-striking Doser's fault-plane solution (DO2) is not in agreement with the NW–SE orientation of the regional structures, the Marañon Thrust and Fold Belt. The test that yields the best numerical solution is given by the local Quiches tensor having a N27°E-trending extension because all the deviations (t, s) are lower than 10° (see the histogram on Fig. 11e). These results permit us to suggest that, while the regional extensional direction in the High Andes of north-central Peru trends N11° ± 10°E, the stress may be slightly reoriented on a N27°E-trending direction in the Quiches region as a result of the proximity of regional Western Cordillera structures, i.e., the Marañon Thrust and Fold Belt.

Normal Fault Geometry

Around Quiches, the surface NW–SE-striking fault has a 55-65°SW dip. But seismological data (Doser, 1987) show that the 1946 Ancash earthquake was generated at a depth of 15 to 17 km on a low angle fault plane dipping at 30° ± 10°SW. In fact, the open fissures and the small grabens locally observed at the toe of the fault scarps do indicate a rapid decrease of fault plane dip versus depth; they support a bifurcation between the superficial high-angle and deep low-angle dip. This suggests that the Quiches 63°SW-dipping surface rupture corresponds to a Tertiary small ramp fault that is connected at shallow depth with a Tertiary thrust plane of the Marañon Thrust and Fold Belt (Fig. 12). This interpretation of the superficial Quiches fault as a Tertiary ramp is supported by the observation of reverse striations on the fault plane, which

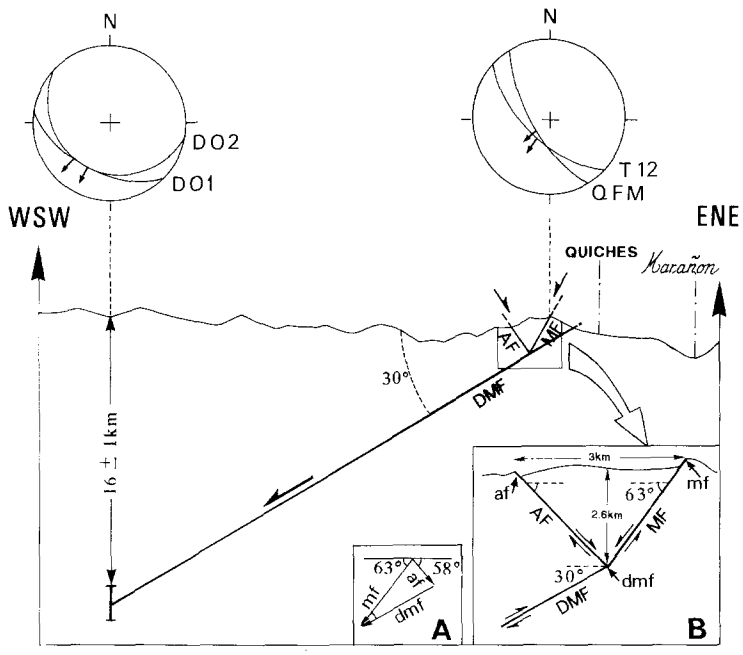


FIG. 12. Sketch cross-section through the Quiches fault constructed from seismic (Doser, 1987) and surface data obtained from the earthquake in 1946. This cross section shows the about 60°SW-dipping surface antithetic and synthetic ruptures connected at depth with an old thrust plane dipping 30°SW. Same symbols as on Figure 11. AF: antithetic fault; MF: major fault. (a) Geometric relationship between the dip slips on the faults; in accordance with King *et al.*'s model (1984), we calculated the dip-slip component at depth on the major fault (dmf), which depends of the dip-slip components on the antithetic (af) and synthetic (mf) surface fault planes. (b) Detailed cross section of the near surface Quiches faults.

indicates that the superficial fault has acted as a reverse fault prior to the normal slip (see the section on Quiches Fault Kinematic History).

Several authors (Armstrong, 1972; Royse *et al.*, 1975; McDonald, 1976; Zoback *et al.*, 1981; Anderson *et al.*, 1983; Stewart, 1983; Smith and Bruhn, 1984; Wallace, 1984; Malavieille, 1987) noted in the Basin and Range, the same relation between some Miocene normal faults and older thrust planes. In the western United States, the Neogene crustal extension occurred in the root zone of some former Laramide thrusts that was reactivated during Miocene normal faulting; one example is the Wasatch fault (e.g., Smith and Bruhn, 1984). These low-angle fault planes are connected with steeply dipping surface faults. Similar geometries have been observed in the Corinth Gulf (Greece) during the 1981 earthquake (Jackson *et al.*, 1982; King *et al.*, 1984) and in the Apennines (Italy) during the 1980 Irpinia earthquake (Westaway and Jackson, 1987) where active normal faulting activated steeply dipping surface faults connected with low-angle fault planes at depth. Similarly in the Peruvian High Andes, we have demonstrated that the Mio-Pliocene and Quaternary extensional tectonics have reactivated Tertiary reverse ramps of the Andean structure (Bellier *et al.*, 1989b) and, in this study, that the present-day extensional tectonics is reactivating Tertiary thrust fault planes of the Marañon Thrust and Fold Belt.

Doser (1987) has observed a complex rupture process for the 1946 earthquake that agrees with our hypothesis on the complexity of the fault plane. The waveforms were best modeled by a source consisting of two major and two minor

ruptures (see on Fig. 6 in Doser, 1987). A complementary study confirms that the rupture was complex, consisting of at least two major pulses of energy release (D. Doser, personal comm.). In agreement with Doser's study, we demonstrate that the geometry of the Quiches fault is complex (Fig. 12) with a superficial mean 63°SW-dipping major rupture, a mean 58°NE-dipping anthitetic rupture, and a deep 30°SW-dipping major fault plane. According to King *et al.*'s (1984) observations on the geometry of the Corinth Gulf (Greece), it can be supposed that the high-angle anthitetic and synthetic faults were connected at depth with the low-angle dipping major fault. This geometry implies that the high-angle faults are connected at about 2.6 km depth with the low-angle fault (Fig. 12a). In addition, the dip-slip component at depth on the major 30°-dipping fault plane ([dmf] on Fig. 12a and b) differs from the dip-slip component on the surficial synthetic 63°-dipping fault ([mf] on Fig. 12a and b). The dip-slip component (dmf) depends on the dip-slip components of the synthetic (mf) and antithetic (af) fault planes (Fig. 12a and b). We have calculated two dip-slip values on the fault plane at depth. First, considering maximum surficial dip slips mf = 3.5 m and af = 1.7 m, the maximum hypothesis gives a maximum dip-slip component at depth dmf = 3 m. Then, considering minimum surficial dip slips mf = 1.5 m and af = 0.8 m, the minimum hypothesis gives a minimum dip-slip component at depth dmf = 1.7 m.

Moment Magnitude of the 1946 Earthquake

The fault geometry (Fig. 12) allows a rough estimation of the seismic moment, and thus of the magnitudes of the 1946 earthquake, that can be compared with the moment and magnitude given by Doser (1987). Seismic moment is defined as $M_0 = \mu DLh$, and moment magnitude as $M_w = (\log M_0 - 16.1)/1.5$ (Brune, 1968; Hanks and Kanamori, 1979; Vassiliou and Kanamori, 1982; Kanamori, 1983) where μ (the shear modulus) = 3×10^{11} dyne $\cdot$ cm^{-1}, D (the mean fault displacement) = 1.7 to 3 m, L (the fault length) = 21 km, and h is the rupture dimension along the fault-plane such as $h = d/\sin P$; according to Doser (1987), d (the focal depth) = 15 to 17 km and P (the mean fault-plane dip) = 30°. These different parameters allow us to calculate a mean seismic moment $M_0 = 4.7 \pm 1.3\ 10^{26}$ dyne $\cdot$ cm^{-1}($4.7 \pm 1.3\ 10^{19}$N $\cdot$ m^{-1}) corresponding to a moment magnitude $M_w = 7.0 \pm 0.1$, which is close to the value of $M_w = 6.8$ given by Doser (1987). We suspect this indicates that most of the 21-km-long Quiches fault was activated during the 1946 earthquake and that the gap in surface rupture corresponds to an area where the seismic rupture failed to propagate up to the surface, or splayed out or steped over to a neighboring structure.

Conclusion

The studies of the 10 November 1946 Ancash earthquake demonstrate the usefulness of field geological approaches to resolve problems in the seismological study of events from the early instrumental era. Particularly when seismological data are of poor quality, a neotectonic analysis helps to constrain the seismic slip vector. The 1946 Ancash earthquake produced a surface faulting along the Quiches normal fault, which is characterized by 1- to 3.5-m-high scarps that displace Holocene moraines and Mesozoic limestones and sandstones. These NW–SE-striking and 63°SW-dipping surface ruptures appear to reactivate a Tertiary thrust. This normal-slip fault shows geometrical similarities with some Laramide thrusts planes reactivated by the Miocene extension of

the Basin and Range province and with active normal faulting in the Apennines (Italy) and in the Corinth Gulf (Greece).

Structural analysis shows that the Holocene normal movement of the Quiches fault has occurred with a minor left-lateral strike-slip component, as has also been observed along the Cordillera Blanca fault zone (Bonnot, 1984; Bonnot *et al.*, 1988). The state of stress deduced from the kinematic analysis of the 1946 slip vectors measured on the major and minor fault planes corresponds to an extensional deviatoric stress tensor characterized by a horizontal NNE–SSW-trending $\sigma 3$ axis (σH min), a horizontal WNW–ESE-trending $\sigma 2$ axis (σH max), and a vertical $\sigma 1$ axis (σzz). This local orientation of $\sigma 3$ (N27°E) is similar to that (N11° ± 10°) of the regional state of stress in the Western Cordillera of Northern and Central Peru, although slightly rotated toward the East. Both these stress tensors can explain the 1946 Quiches focal mechanism obtained by Doser (1987).

The minimum time span between the two last major events with magnitude M_w 6.8 to 7 (i.e., between the 1946 event and the Late Pleistocene event evidenced by the trench analysis) permit us to suggest that the average recurrence interval for surface faulting earthquakes on the Quiches fault is more than 13,000 ± 1,000 years. Correspondingly, the approximate rate of dip slip on the fault is less than 0.27 ± 0.02 mm/yr.

The north-central Peruvian Andes are situated above a flat subducting oceanic slab (Stauder, 1975; Barazangi and Isacks, 1979; Cross and Pilger, 1982; Bevis and Isacks, 1984). In this region, the state of stress in the upper crust, which explains the active deformation in the High Andes of Peru (Mercier, 1981; Dalmayrac and Molnar, 1981; Suarez *et al.*, 1983, Sébrier *et al.*, 1985, 1988; Cabrera *et al.*, 1987; Schwartz, 1988; Bonnot *et al.*, 1988; Bellier, 1989), results from the interaction between the body forces produced by the Andean topography and the boundary forces resulting from the convergence between the South American and Nazca plates (Sébrier *et al.*, 1985, 1988). Thus, the gravitational body forces acting on the high plateau of the Andes are in part responsible for the High Andes' present-day extensional tectonics, a situation similar to those of Tibet (e.g., Tapponnier and Molnar, 1977; Mercier *et al.*, 1987; Dewey, 1988) and of the Cenozoic Basin and Range (e.g., Coney and Harms, 1984; Glazner and Bartley, 1985; Malavieille, 1987; Dewey, 1988), where extension acts on overthickened crusts involving uplift and heating. In the other hand, as in the Basin and Range Province, extensional tectonics in the Quiches zone reactivates preexisting thrust fault planes.

Acknowledgments

This work has been realized within the Cooperative Research Program between the Institut Français de Recherche Scientifique pour le Developpement en Coopération (ORSTOM) and the Instituto Geofísico del Perú (I.G.P.). This study was also supported by the Institut National des Sciences de l'Univers (INSU). Thoughtful and constructive reviews by S. Pezzopane and K. W. Hudnut greatly improved the paper. Special thanks are due to D. Odekirk, I. Sharp, P. Vergely, D. P. Schwartz, and D. I. Doser for reading the manuscript; D. I. Doser's and D. P. Schwartz' additional comments concerning, respectively, the 1946 Quiches earthquake and the paleoseismicity analyses were gratefully appreciated.

References

Anderson, E. R., M. L. Zoback, and G. Thompson (1983). Implications of selected sub-surface data on the structural form and evolution of some basins in the northern Basin and Range Province, Nevada and Utah, *Geol. Soc. Am. Bull.* **94**, 1055–1072.

Armstrong, R. L. (1972). Low-angle (denudation) faults, hinterland of the Servier orogenic belt, eastern Nevada and western Utah, *Geol. Soc. Am. Bull.* **84**, 1729-1754.

Barazangi, M. and B. L. Isacks (1979). Subduction of the Nazca Plate beneath Peru: evidence from spatial distribution of earthquakes, *Geophys. Roy. Astr. Soc.* **57**, 537-555.

Bellier, O. (1989). Tectonique en extension et changement d'états de contraintes cénozoïque en domaine intra-continental: exemple des bassins intra-cordillérains des Hautes Andes (Nord Pérou) et du graben de la Wei He (Chine du Nord), *Thesis Univ. d'Orsay*, 296 pp.

Bellier, O., J. Macharé, and M. Sébrier (1989a). Extensión actual del Nor Peru: estudio de la falla activa de Chaquilbamba (Norte del departamento de La Libertad, Perú), *Bol. Soc. Geol. Perú* **80**, 1-12.

Bellier, O., M. Sébrier, E. Fourtanier, F. Gasse, and I. Robles (1989b). Neogene and Quaternary geodynamic evolution of an intra-cordilleran basis: the Namora basin in Northern Peruvian Andes, *Annales Tectonicae* **3**, 2, 77-98.

Bevis, M. and B. L. Isacks (1984). Hypocentral trend surface analysis: probing the geometry of the Benioff zones, *J. Geophys. Res.* **89**, (B7), 6153-6170.

Birkeland, P. W., D. T. Rodbell, and S. K. Short (1989). Radiocarbon dates on deglaciation, Cordillera Central, northern Peruvian Andes, *Quat. Res.* **32**, 111-113.

Bonnot, D. (1984). Néotectonique et Tectonique active de la Cordillére Blanche et du Callejon de Huaylas. Andes Nord peruviennes, *Thèse Univ. d'Orsay*, 115 pp.

Bonnot, D., M. Sébrier, and J. L. Mercier (1988). Evolution geodynamique plio-quaternaire du bassin intra-cordillerain du Callejon de Huaylas et de la region de la Cordillère Blanche, Pérou, *Geodynamique* **3**, 57-83.

Brune, J. (1968). Seismic moment, seismicity and rate of slip along major fault zones, *J. Geophys. Res.* **73**, 777-784.

Bucknam, R. C. and R. Anderson (1979). Estimation of fault-scarp ages from a scarp-height-slope-angle relationship, *Geology* **7**, 11-14.

Cabrera, J. (1988). Néotectonique et sismotectonique dans la Cordillère andine au niveau du changement de géométrie de la subduction: la région de Cuzco (Pérou), *Thèse Univ. d'Orsay*, 275 pp.

Cabrera, J., M. Sébrier, and J. L. Mercier (1987). Active normal faulting in high plateaus of central Andes: the Cuzco region (Peru), *Annales Tectonicae* **1**, 2, 116-138.

Carey, E. (1979). Recherche des directions principales de contraintes associées au jeu d'une population de failles, *Rev. Géol. Dyn. Géogr. Phys.* **21**, 57-66.

Carey, E. and B. Brunier (1974). Analyse théorique et numérique d'une modèle mécanique élémentaire appliqué à l'étude d'une population de failles, *C. R. Hebd. Séances Acad. Sci.* **279**, 891-894.

Clapperton, C. M. (1981). Quaternary glaciations in the Cordillera Blanca, Peru and the Cordillera Real, Bolivia, *Rev. Cent. Interam. Fotointerpretación* **6**, 93-111.

Coney, P. J. and T. A. Harms (1984). Cordilleran metamorphic core complexes: cenozoic extensional relics of Mesozoic compression, *Geology* **12**, 550-554.

Cross, T. A. and R. H. Pilger (1982). Controls of subduction geometry, location of magmatic arc and tectonics of arc and back-arc regions, *Geol. Soc. Am. Bull.* **93**, 545-562.

Dalmayrac, B. and P. Molnar (1981). Parallel thrust and normal faulting in Peru and constraints on the state of stress, *Earth Planet. Sci. Lett.* **55**, 473-481.

Deverchère, J. (1988). Extension crustale dans un contexte de convergence de plaques: l'exemple des Andes du Pérou central contraint par des données sismotectoniques, *Thèse Univ. d'Orsay*, 234 pp.

Deverchère, J., C. Dorbath, and L. Dorbath (1989). Extension related to high topography: results from a microearthquake survey in the Andes of Peru and tectonic implications, *Geophys. J. Int.* **98**, 281-292.

Dewey, J. F. (1988). Extensional collapse of orogens, *Tectonics* **7**, 6, 1123-1139.

Doser, D. I. (1987). The Ancash, Peru, earthquake of 1946 November 10: Evidence for low-angle normal faulting in the high Andes of northern Peru, *Geophys. J. R. Astr. Soc.* **91**, 57-71.

Glazner, A. F. and J. M. Bartley (1985). Evolution of lithospheric strength after thrusting, *Geology* **13**, 42-45.

Hancock, P. L. (1985). Brittle microtectonics: principles and practice, *J. Struct. Geol.* **7**, 3/4, 437-457.

Hanks, T. C. and H. Kanamori (1979). A moment magnitud scale, *J. Geophys. Res.* **84**, 2348-2350.

Hanks, T. C., R. C. Bucknam, K. R. Lajoie, and R. E. Wallace (1984). Modification of wave-cut and faulting-controlled landforms, *J. Geophys. Res.* **89**, B7, 5771-5790.

Hansen, B. C. S., H. E. Wright, Jr., and J. P. Bradbury (1984), Pollen studies in the Junin area, central Peruvian Andes, *Geol. Soc. Am. Bull.* **12**, 1454–1465.

Heim, A. (1949). Observaciones geológicas en la región del terremoto de Ancash de Noviembre de 1946, *Soc. Geol. Perú*, Vol. Jub. Part **2**, Fasc. 6, 28 pp.

Hodgson, J. H. and P. C. Bremner (1953). Direction of faulting in the Ancash, Peru, earthquake of November 10, 1946, from teleseismic evidence, *Bull. Seism. Soc. Am.* **43**, 121–125.

Jackson, J. A., J. Gagnepain, G. Houseman, G. King, P. Papadimitriou, C. Soufleris, and J. Virieux (1982). Seismicity, normal faulting and the geomorphological evolution of the Gulf of Corinth, (Greece): the Corinth earthquakes of February and March 1981, *Earth Planet. Sci. Lett.* **57**, 377–397.

Kanamori, H. (1983). Magnitude scale and quantification of earthquakes, *Tectonophysics* **93**, 185–199.

King, G., Z. Ouyang, P. Papadimitriou, A. Deschamps, J. Gagnepain, G. Houseman, J. Jackson, C. Soufleris, and J. Virieux (1984). The evolution of the Gulf of Corinth (Greece): an aftershock study of the 1981 earthquake, *Geophys. J. R. Astr. Soc.* **80**, 677–693.

McDonald, R. E. (1976). Tertiary tectonics and sedimentary rocks along the transition: Basin and Range Province to Plateau and Thrust Belt Province, Utah, in *Geology of the Cordilleran Hingeline*, J. G. Hill (Editor), Rocky Mountain Association of Geologists, 281–317.

Malavieille, J. (1987). Kinematics of compressional and extensional ductile shearing deformation in a metamorphic core complex of the northeastern Basin and Range, *J. Struct. Geol.*, **9**, 541–554.

Mattauer, M. (1973)Les déformations des matériaux de l'Ecorce Terrrestre, Hermann (Editor), Paris, 494.

Mégard, F. (1984). The Andean orogenic period and its major structures in central and northern Peru, *J. Geol. Soc. Lond.* **141**, 893–900.

Meghraoui, M., H. Philip, F. Albarede, and A. Cisternas (1988). Trench investigations through the trace of the 1980 El Asnam thrust fault: evidence for paleoseismicity, *Bull. Seism. Soc. Am.* **78**, 979–999.

Mercer, J. H. (1983). Late Cainozoic glacial variations in South America south of the equator, in *Late Cainozoic Palaeoclimates of the Southern Hemisphere*, J. C. Vogel (Editor), South Africa, 520 pp.

Mercer, J. H. and O. Palacios (1977). Radiocarbon dating of the last glaciation in Peru, *Geology* **5**, 600–604.

Mercier, J. L. (1981). Extensional-compressional tectonics associated with the Aegean arc: comparison with the Andean Cordillera of south Peru-north Bolivia, *Phil. Trans. R. Soc. London. A* **300**, 337–355.

Mercier, J. L., N. Mouyaris, C. Simeakis, T. Roundoyannis, and C. Angelidhis (1979). Intra-plate deformation: a quantitative study of the fault activated by the 1978 Thessaloniki earthquakes, *Nature* **278**, 5699, 45–48.

Mercier, J. L., E. Carey-Gailhardis, N. Mouyaris, C. Simeakis, T. Roundoyannis, and C. Angelidhis (1983). Structural analysis of recent and active faults and regional state of stress in the epicentral area of the 1978 Thessaloniki earthquakes (Northern Greece), *Tectonics* **2**, 577–600.

Mercier, J. L., R. Armijo, P. Tapponnier, E. Carey, and T. L. Han (1987). Change from late Tertiary compressional tectonics to Pleistocene extensional tectonics in Tibet subsequent to the India-Asia collision, *Tectonics* **6**, 275–304.

Nash, D. B. (1980). Morphologic dating of degraded normal fault scarps, *J. Geology* **88**, 353–360.

Pilger, R. H. (1984). Cenozoic plate kinematics, subduction and magmatism: South american Andes, *J. Geol. Soc. Lond.* **141**, 793–202.

Philip, H. and M. Meghraoui (1983). Structural analysis and interpretation of the surface deformations of the El Asnam earthquake of October 10, 1980, *Tectonics* **2**, 17–49.

Richter, C. F. (1958). *Elementary Seismology*, W. H. Freeman, San Francisco, 768 pp.

Royse, F., Jr., M. A. Warner, and D. L. Reese (1975). Thrust belt structural geometry and related stratigraphic problems, in *Deep Drilling Frontiers of the Central Rocky Mountains*, D. W. Bolyard (Editor), Rocky Mountain Association of Geologists, Denver, 41–54.

Schwartz, D. P. and K. J. Coppersmith (1984). Fault behavior and characteristic earthquakes: examples from the Wasatch and San Andreas fault zones, *J. Geophys. Res.* **89**, 5681–5698.

Schwartz, D. P. (1988). Paleoseismicity and neotectonics of the Cordillera Blanca fault zone, Northern Peruvian Andes, *J. Geophys. Res.* **93**, 4712–4730.

Sébrier, M., D. Huamán, J. L. Blanc, J. Macharé, D. Bonnot, and J. Cabrera (1982). Observaciones acerca de la Neotectónica del Peru, *Inf. Pro. SISRA, CERESIS, Lima*, 440 pp.

Sébrier, M., J. L. Mercier, F. Mégard, G. Laubacher, and E. Carey-Gailhardis (1985). Quaternary

normal and reverse faulting and the state of stress in Central Andes of South Peru, *Tectonics* **4**, 739-780.

Sébrier, M., J. L. Mercier, J. Macharé, D. Bonnot, J. Cabrera, and J. L. Blanc (1988). The state of stress in an overriding plate situated above a flat slab: the Andes of Central Peru, *Tectonics* **7**, 895-928.

Sébrier, M. and P. Soler (1990). Tectonics and magmatism in the Peruvian Andes from Late Oligocene to Present, in *Andean Magmatism and its Tectonic Setting*, *G.S. A. Special Paper* (in press).

Sieh, K. E. and R. H. Jahns (1984). Holocene activity of the San Andreas fault at Wallace Creek, California, *Bull. Seism. Soc. Am.* **95**, 883-896.

Silgado, E. (1947). Datos sismológicos del Perú, 1946, *Bol. Inst. Geol. Perú* **7**, 32 pp.

Silgado, E. (1948). Datos sismológicos del Perú, 1947, *Bol. Inst. Geol. Perú* **11**, 32 pp.

Silgado, E. (1949). Datos sismológicos del Perú, 1948, *Bol. Inst. Geol. Perú* **13**, 35 pp.

Silgado, E. (1951). The Ancash, Peru, earthquake of November 10, 1946, *Bull. Seism. Soc. Am.* **41**, 2, 83-100.

Silgado, E. (1957). Datos sismológicos del Perú, 1952-1955, *Bol. Inst. Geol. Perú* **24**, 71 pp.

Silgado, E. (1978). Historia de los sismos más notables ocurridos en el Perú (1513-1974), *Bol. Inst. Geol. y Min. Perú* **3**, 130 pp.

Smith, R. B. and R. L. Bruhn (1984). Intraplate extensional tectonics of the eastern Basin-Range: inferences on structural style from seismic reflection data, regional tectonics and thermal-mechanical models of brittle-ductile deformation, *J. Geophys. Res.* **89**, 5733-5762.

Stewart, J. H. (1983). Cenozoïc structure and tectonics of the northern Basin and Range province, California, Nevada, and Utah, *Geoth. Resource Council, Special Report* **13**, 25-40.

Stauder, W. (1975). Subduction of Nazca plate under Peru as evidenced by focal mechanisms and by seismicity, *J. Geophys. Res.* **80**, 1053-1064.

Suarez, G., P. Molnar, and B. Burchfiel (1983). Seismicity, fault plane solutions, depth of faulting, and active tectonics of the Andes of Peru, Ecuador and southern Colombia, *J. Geophys. Res.* **88**, 10403-10428.

Swan, F. H., D. P. Schwartz, and L. S. Cluff (1980). Recurrence of moderate to large magnitude earthquakes produced by surface faulting on the Wasatch fault zone, Utah, *Bull. Seism. Soc. Am.* **70**, 1431-1462.

Tapponnier, P. and P. Molnar (1977). Active faulting and tectonics in China, *J. Geophys. Res.* **82**, 2905-2930.

Vassilou, M. S. and H. Kanamori (1982). The energy release in earthquakes, *Bull. Seism. Soc. Am.* **72**, 372-387.

Vergely P., W. Sassi, and E. Carey-Gailhardis (1987). Analyse graphique des failles á l'aide de focalisations de stries, *Bull. Soc. Géol. France* **3**, 395-402.

Wallace, R. E. (1977). Profiles and ages of young fault scarps, north-central Nevada, *Geol. Soc. Am. Bull.* **88**, 1267-1281.

Wallace, R. E. (1984). Fault scarps formed during the earthquakes of October 2, 1915, in Pleasant Valley, Nevada, and some tectonic implications, *U.S. Geol. Surv. Profess. Paper 1274-A*, 33 pp.

Watson, G. S. (1960). More significance tests on the sphere, *Biometrika*, **47**, 87-91.

Westaway, R. and J. Jackson (1987). The earthquake of 1980 November 23 in Campania-Basilica (southern Italy), *Geophys. J. R. Astr. Soc.* **90**, 375-443.

Wilson, J. J., L. Reyes, and J. Garayar (1967). Geologiá de los Cuadrańgulos de Mollebamba, Tayabamba, Huaylas, Pomabamba, Carhuaz y Huari, *Bol. Serv. Geol. Min., Lima* **16**, 95.

Wright, H. E. (1984). Late glacial and late Holocene moraines in the Cerros Cuchpanga, central Peru, *Quat. Res.* **21**, 275-285.

Zoback, M. L., R. E. Anderson, and G. A. Thompson (1981). Cenozoic evolution of the state of stress and style of tectonism of the Basin and Range province of the western United States, *Phil. Trans. R. Soc. Lond. A* **300**, 407-434.

URA CNRS Geophysique et Geodynamique Interne
Bat. 509
91405 Orsay Cedex, France
(O.B., M.S., J.L.M.)

ORSTOM, U.R. 105
213 rue Lafayette
75 480 Paris Cedex 10, France
(J.F.D.)

Manuscript received 11 December 1989